Optica Applicata, Vol. XLII, No. 3, 2012
DOI: 10.5277/oa120307

Application of fiber Bragg gratings for strain measurement in historic textiles and paintings on canvas

WITOLD ZAWADZKI[1], MARCIN BARTOSIK[1], KRZYSZTOF DZIERŻĘGA[1*], ŁUKASZ BRATASZ[2], MICHAŁ ŁUKOMSKI[3], ELIZABETH PEACOCK[4, 5]

[1]Marian Smoluchowski Institute of Physics, Jagiellonian University, ul. Reymonta 4, 30-059 Kraków, Poland

[2]The National Museum in Kraków, al. 3 Maja 1, 30-062 Kraków, Poland

[3]Jerzy Haber Institute of Catalysis and Surface Chemistry, Polish Academy of Sciences, ul. Niezapominajek 8, 30-239 Kraków, Poland

[4]Museum of Natural History and Archaeology, Norwegian University of Science and Technology, NO-7491 Trondheim, Norway

[5]Department of Conservation, University of Gothenburg, Gothenburg, Sweden

[*]Corresponding author: krzysztof.dzierzega@uj.edu.pl

The aim of this work was to evaluate the applicability of optical fiber Bragg grating (FBG) sensors to the monitoring of deformation in historical textiles and paintings on canvas. Fibers with a ceramic coating were selected for strain investigation in textiles due to both their almost perfect strain transfer and much shorter relaxation times compared to fibers with an acrylate coating. FBG sensors were attached to fabrics in a non-destructive manner using specially designed magnetic clamps. Local strain measurements using these sensors were consistent with general strains measured using either a universal testing machine (UTM) or a laser triangulator when varying external load or relative humidity. However, strain magnitudes measured by the different methods were comparable only after correction for the influence of the fiber on the textile under study. Strain measurements in model paintings on canvas were carried out using uncoated fibers embedded in the gesso layers on the canvas.

Despite some drawbacks, the FBG sensors were found to be useful in monitoring strain in historic textiles and consequently, for the assessment of environmental risk of these works-of-art.

Keywords: fiber Bragg garting, strain sensor, historic textiles, paintings.

1. Introduction

Historic textiles such as tapestries, carpets, kilims, banners and liturgical vestments, and especially paintings on canvas are appreciable part of museum collections. During

long periods of storage and exhibition they can be subjected to multiple environmental agents/factors including temperature, humidity or light that bring about degradation through chemical and physical processes. Moreover, since textiles are frequently large and consequently, heavy, loading imposed by their own weight is considered a possible factor responsible for their deterioration, as well. Their damage may be accelerated by the simultaneous action and mutual interaction of several of the above-mentioned factors.

Despite the existence of ample literature presenting research on textile degradation, assessment and comparison of different methods and techniques of conservation and exhibition of textiles and paintings on canvas have often been based on criteria determined from long-term practical observations and experience acquired by curators and conservators. Based on the common practice of museums, reflected in conservation guidelines and loan policies, climate induced deformations in textiles are perceived as one of the most important reasons for damage in textile collections. On the other hand climate stabilisation of storage and exhibition rooms belongs to the most energy consuming one's. Therefore, expensive conservation strategies should be avoided if not really necessary.

The application of fiber Bragg gratings (FBGs) for monitoring strain in woven textiles has been investigated by YE *et al*. [1, 2]. Both silica and polymer optical fiber (POF) gratings were evaluated, and two different adhesive systems (two-part epoxy Araldite 2015 and polyvinyl acetate (PVA) based adhesive Mowilith DMC2) were tested for attaching the FBG sensors to a tapestry. The performance of these sensors was validated by comparison with the results of a non-contact digital image correlation (DIC) study of the same textile. It has been demonstrated that POFs, which are constructed of PMMA (polymethylmethacrylate), provide a better strain transfer coefficient. Furthermore, when adhered with PVA, they produce less structural reinforcement than silica fibers. This is readily explained by the much lower (1.3 GPa) Young's modulus of PMMA compared to silica (31.5 GPa). Unfortunately, the high attenuation of PMMA in the visible and near-infrared makes the structure of the sensor head more complex and much less robust. Moreover, high (up to 8 nm for RH change of 100%) relative humidity sensitivity of polymer FBGs makes strain measurements unreliable in variable ambient climatic conditions. Furthermore, since the technology of FBG inscription in polymers is not yet fully developed, these gratings are characterized by short-term stability, not longer than several months [3].

Another aspect of the application of FBGs to textiles and historic textiles in particular, is related to their attachment. Bonding the fiber to the specimen is a common technique that produces excellent results in many fields of industry and technology; however, such a technique is unacceptable in the case of museum objects. Therefore, a different method of fiber–textile contact is needed.

In this work, a study was carried out of the performance of the standard silica FBG to monitor strain variations in woolen textiles and paintings on canvas. Two types of fibers: with acrylate and organic modulated ceramic (ORMOCER) coating, were

investigated while incorporating the fiber with textile was achieved using specially designed magnetic clamps. Investigation results of the effect of temperature, humidity, load and the size of clamps on the sensor response are presented and compared with the results of the laser triangulation method.

2. Fiber Bragg grating sensor

A fiber Bragg grating is a special optical fiber whose refractive index of the core varies periodically. Such periodicity is usually obtained by irradiating the UV-sensitive fiber with a spatially modulated intense UV laser beam [4]. When spectrally broad light is injected into the fiber and interacts with the Bragg grating, the wavelength is reflected in a narrow band (~0.1 nm). If the grating pitch is Λ, the resonance condition for the reflected wavelength is given by:

$$\lambda_B = 2n_{\text{eff}}\Lambda \tag{1}$$

where λ_B is the so-called Bragg wavelength and n_{eff} is the effective refractive index of the fiber core. Any physical parameter that changes the grating pitch or the fiber core refractive index can produce a shift in the Bragg wavelength which can be measured by different optical intensity-based or interferometric methods. The two main parameters affecting λ_B are strain and temperature and the change of the Bragg wavelength $\Delta\lambda_B$ is

$$\frac{\Delta\lambda_B}{\lambda_B} = (1 - p_e)\varepsilon + (\alpha_\Lambda - \alpha_n) \tag{2}$$

The first term on the right-hand-side describes contribution of the elongation with ε being the applied strain and p_e the photoelastic coefficient. The second term is the thermal contribution, where α_Λ is the thermal expansion coefficient of the fiber while α_n is the thermal modulation coefficient of its refractive index. The information about strain or temperature change is measured by the change in wavelength and not in the light intensity. The wavelength is independent of losses in the fiber, connections between optical components of the fiber sensor and of fluctuations of intensity in the light source. Moreover, a number of gratings – with different Bragg wavelengths – can be inscribed on the same fiber, thus facilitating simultaneous strain detection in different parts of the object under investigation using one and the same system.

3. Experiment

Silica FBGs with acrylate (aFBG) and ceramic (cFBG) coatings were investigated as strain sensors; their specifications are presented in Table 1. In spite of similarities in the fiber core diameter and cladding as well as grating length, aFBG and cFBG

T a b l e 1. Specifications of uncoated fibers with FBGs used in this work.

	aFBG*	cFBG*
Core diameter [μm]	9	6
Cladding diameter [μm]	125	125
Buffer diameter [μm]	250	195
FBG length [mm]	10	8
Reflectivity [%]	80	17
FWHM [nm]	0.3	0.1
Max strain [%]	0.9	5
Temp. sens. [pm/°C]	11	10
Humid. sens. [pm/% RH]	0.28	1.3
Young's modulus [GPa]	31.5	31.5

*FBGs provided by SmartFibres (acrylate) and FBGS Technologies (ceramic).

differ significantly in their reflectivities and strain-sensing range. The maximum strain-sensing value of cFBG is 5% (compared to 0.9% of aFBG) which is not much less than 13% achievable with POFs [5, 6].

Figure 1 shows the sensing arrangement for the fiber Bragg grating system. It consists of a 50 nm broad superluminescent diode (SLED) with the central wavelength around 1540 nm. The light beam from the SLED passes through an optical isolator and is introduced into a 3-port optical circulator with an FBG attached to a single end. The reflected spectrum from the FBG is monitored using a grating spectrometer equipped with a photodiode array (I-MON interrogator by Ibsen Photonics). The spectral resolution of the measured wavelengths was better than 1 pm corresponding approximately to 1 με, *i.e.*, 0.0001%. In the present study, several FBGs with acrylate and ceramic coatings were tested with nominal Bragg wavelengths in the spectral range between 1539 nm and 1556 nm.

The experimental test textile was a 1 mm thick woolen tapestry from the first half of the 20th century constructed of weft yarns made from wool and warp yarns made

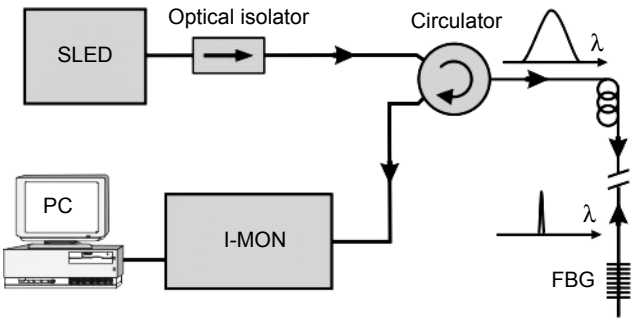

Fig. 1. Experimental arrangement for the fiber Bragg gratings system (detailed description in the text).

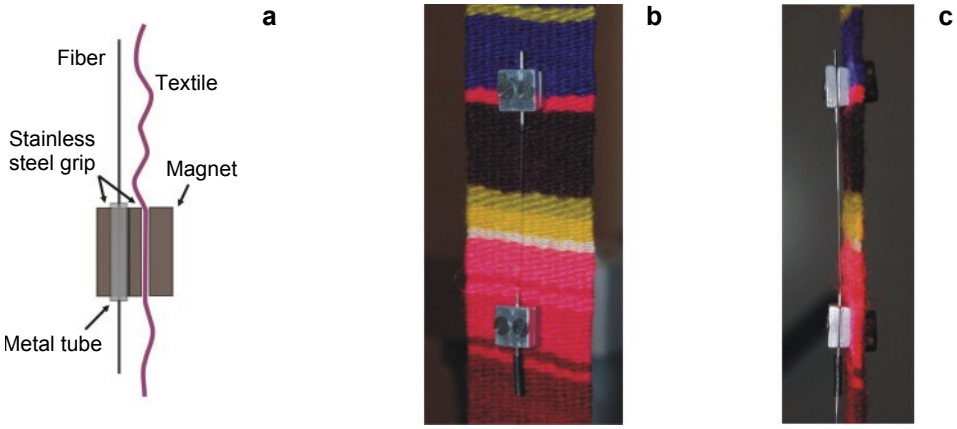

Fig. 2. System to attach the fiber Bragg grating sensor to the test textile using magnetic clamps: scheme of the magnetic clamp (**a**). Front (**b**) and side (**c**) views of the clamp fastened to the textile.

of flax. The textile had 20 yarns/cm and 12 yarns/cm along the weft and warp directions, respectively, and its weight was 0.5 kg/m^2.

The FBG sensor head was attached to the test fabric by means of specially developed magnetic clamps shown in Figs. 2. At two sides of the FBG, and 21 mm away from its center, the fiber was bonded into 10 mm-long stainless steel tubes with 0.6 mm outer diameter using cyanoacrylate. These tubes were placed in the groove between two 1-mm thick steel plates (see Fig. 2**b**) which were then tightly bolted together. The size of the plates varied from 20×80 mm^2 to 20×150 mm^2 in order to minimize the influence of the clamps on the strain in the textile sample. Finally, the fiber with metal grips was attached by magnets to the selected part of the textile as illustrated in Figs. 2**a** and 2**c**. The quality of such attachment was verified by periodic stretching the textile under study. No variations of the strain measured by FBG sensor were found from cycle to cycle, which indicated no sliding of the magnetic clamps over the textile surface. All mechanical tests were carried out using a universal testing machine (UTM). A climate chamber was used to study the response of the FBG sensor to variations of microclimate parameters: temperature and relative humidity.

4. Results and discussion

4.1. Strain transfer to the FBG sensor head

The response of the FBGs to an applied strain was studied by mounting each fiber, bonded into a metallic tube, in the grips of the UTM. Figure 3 shows the results of the quasi-static (slow strain variations compared to fiber relaxation) experiments in which the Bragg wavelengths of the aFBG and the cFBG were measured in relation to the strain applied to the fiber by the UTM. Although linear dependence was observed for both sensors, the cFBG was characterized by a larger strain transfer

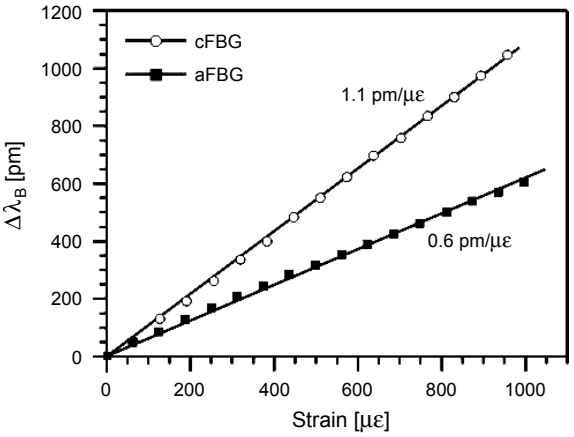

Fig. 3. Variations of the Bragg wavelength during a quasi-static (με/min) test in an UTM. Strain transfers for the aFBG and the cFBG amount to 0.6 and 1.1 pm/με, respectively.

from the coating to the fiber resulting in a strain sensitivity of 1.10(5) pm/με compared to 0.60(4) pm/με for the aFBG. A sensitivity of the bare, uncoated fiber was 1.2 pm/με.

The dynamic response of fiber sensors was studied by means of the UTM quickly stretching and releasing the FBGs at a rate of 1.0 mε/s. The results of this experiment, shown in Fig. 4, indicate time-dependent fiber response with a relaxation time of about 1 min for the aFBG and almost instantaneous response for the cFBG. Based upon the relatively small transfer coefficient of the strain and long relaxation time compared to monitored phenomena, aFBGs were excluded from further investigation.

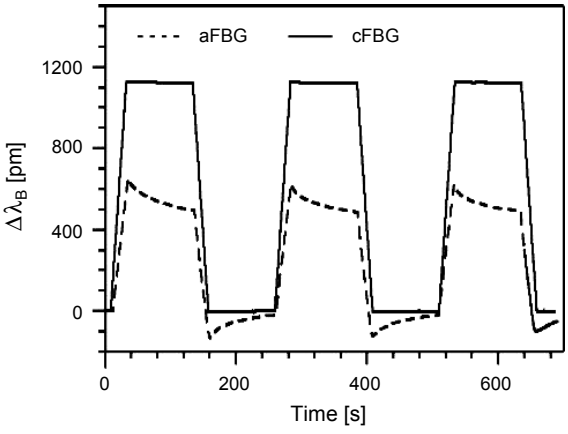

Fig. 4. Relative variations of the Bragg wavelength of the aFBG (dashed line) and the cFBG (solid line) during a dynamic test in the UTM.

4.2. Strain measurements in textile specimens

The performance of the cFBG sensor attached to the textile was evaluated on a series of textile specimens using the UTM. For quasi-static tests, the fiber with the cFBG was fixed to the specimen by means of 80-mm wide magnetic clamps. To study deformation, the textile was then mounted in the UTM and periodically stretched and

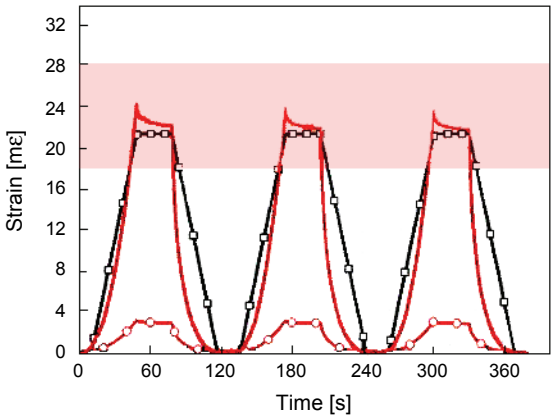

Fig. 5. Strain variations applied by the UTM (□) and recorded by the cFBG sensor (○) attached to the test fabric by means of the magnetic clamps with surface area of 80×20 mm^2. The total length of the sensor was 80 mm and the strain was applied in the weft direction. The solid line represents the strain recorded by the cFBG after correction for fiber interference. The shadowed area corresponds to uncertainty limits including UTM and FBG sensor uncertainties as well as the uncertainty of the determined Young's moduli.

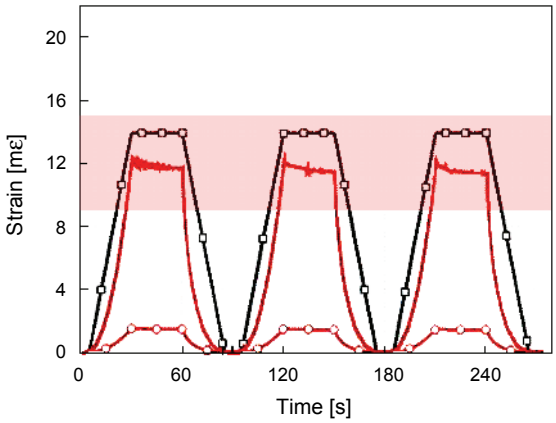

Fig. 6. Strain variations applied by the UTM (□) and recorded by the cFBG sensor (○) attached to the test fabric by means of the magnetic clamps with a surface area of 80×20 mm^2. The total length of the sensor was 80 mm and the strain was applied along the warp direction. The solid line indicates the strain recorded by the cFBG after correction for fiber interference.

released at a rate of 0.22 mm/s with a maximum strain of 22 mε and 14 mε in the weft and the warp directions, respectively. Figures 5 and 6 present strain variations applied by the UTM and measured by the cFBG.

It is apparent that the strain recorded by the cFBG follows the strain applied to the specimen, but at significantly lower amplitude. This effect is repeatable from cycle to cycle, indicating an influence of the sensor head, in particular the fiber, on the textile during testing.

In order to explain the observed discrepancies the system was modeled as consisting of two parts (see Fig. 7) connected in series and loaded with force F. The upper part includes the piece of the textile specimen of the length L_0 equal to the length of the cFBG sensor integrated in parallel. The lower part corresponds to the rest of the textile specimen with the length L_1. The specimen and the cFBG are characterized by the Young's moduli E_1 and E_0 and the cross-sectional areas A_1 and A_0, respectively. Although in general Young's modulus is a quantity varying with strain, in the range of strains being studied (up to 10 mε) it is assumed constant.

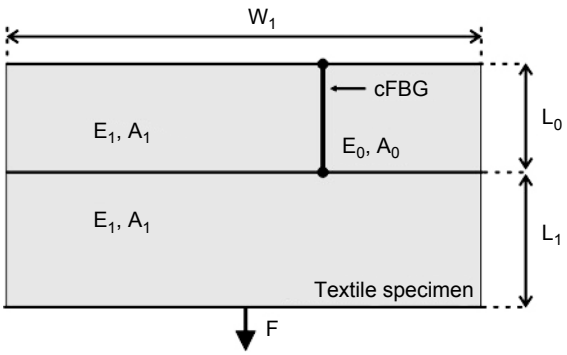

Fig. 7. Model configuration of the specimen and the cFBG loaded by F.

The overall strain applied by the UTM can be written as:

$$\varepsilon_T = \frac{\Delta L_0 + \Delta L_1}{L_0 + L_1} = \varepsilon_1 - (\varepsilon_1 - \varepsilon_0)\frac{L_0}{L_0 + L_1} \tag{3}$$

where $\varepsilon_1 = \Delta L_1/L_1$ and $\varepsilon_0 = \Delta L_0/L_0$ represent the strains of the lower and upper parts, respectively. Using the relation between strain and stress, the lower and upper subsystems can be written as follows:

$$\varepsilon_1 = \frac{F}{A_1 E_1} \tag{4a}$$

$$\varepsilon_0 = \frac{F}{A_1 E_1 + A_0 E_0} \tag{4b}$$

Equations (3) and (4) can be used to relate ε_0 measured by the FBG sensor and applied strains ε_T as

$$\varepsilon_0 = \frac{\varepsilon_T}{1 + \dfrac{A_0}{w_1 d_1}\dfrac{E_0}{E_1}\dfrac{L_0}{L_0 + L_1}} \tag{5}$$

where $w_1 d_1 = A_1$ (w_1 and d_1 denote the width of the magnetic clamp and the thickness of the textile). It is clear that by minimizing the second term in the denominator of Eq. (5) the influence of the sensor head on textile deformation as the result of the cFBG is negligible. Since usually $L_1 \gg L_0$, the latter condition is fulfilled only if $A_1 E_1 \gg A_0 E_0$. Under the experimental conditions $E_0 = 31.5$ GPa, $A_0 = 3.0\times10^{-4}$ cm^2, $L_0 = 4$ cm, $L_1 = 12$ cm, $w_1 = 8$ cm and $d_1 = 1.0$ mm. The most uncertain quantity in the calculations is Young's modulus of the textile. Figure 8 shows a typical stress–strain dependence for the test specimens fixed and then stretched along the weft (warp) direction in the UTM. The calculated Young's modulus for the textile is presented in the same figure. The slope of the stress–strain curve increases with applied strain by one order of magnitude as a result of yarn decrimping at low load. In effect, the overall disturbance of the fabric by the fiber sensor is significantly reduced. It is also evident that the lower the strain the larger the uncertainty of Young's modulus. In the range of textile deformations under investigation, *i.e.*, between 1 and 10 mε, $E_1 \approx 35.7$ N/cm and 60.5 N/cm (per unit width of the textile) were evaluated with uncertainties as high as 50%. Substituting all quantities in Eq. (5), we obtain ε_0 values which are consistent with ε_T within the uncertainty limits (see Figs. 5 and 6).

The performance of the FBG sensor was also investigated using magnetic clamps of different sizes, *i.e.*, of different widths w_1. As was expected, the wider the clamps, the lower the discrepancy between the applied ε_T and measured strains ε_0.

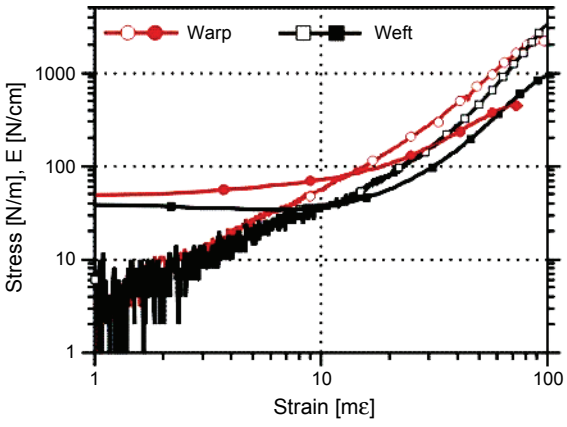

Fig. 8. Measured stress (open symbols) and calculated Young's modulus (full symbols) depending on applied strain for the test fabric stretched in the weft and the warp directions in the UTM.

4.3. Strain measurements in the test textile at variable microclimatic conditions

Relative humidity (RH) is the most important microclimatic parameter that directly impacts the weight of a textile object and its deformation. Studies of RH influence on textile strain were carried out by placing the textile in the climate chamber and by varying the relative humidity in the range between 25% and 70% at constant temperature of 20 °C.

As is shown in Fig. 9, the specimen was mounted vertically and pre-stretched in the weft direction by loading bar of the weight of 633 g. Strain variations in the textile

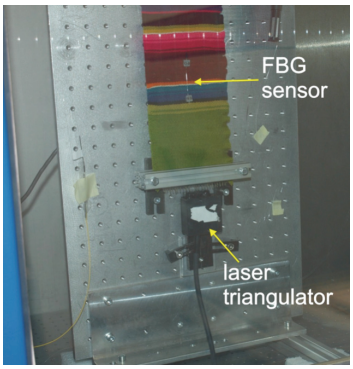

◀ Fig. 9. Experimental setup for strain measurements by FBG sensor and laser triangulator in the climatic chamber.

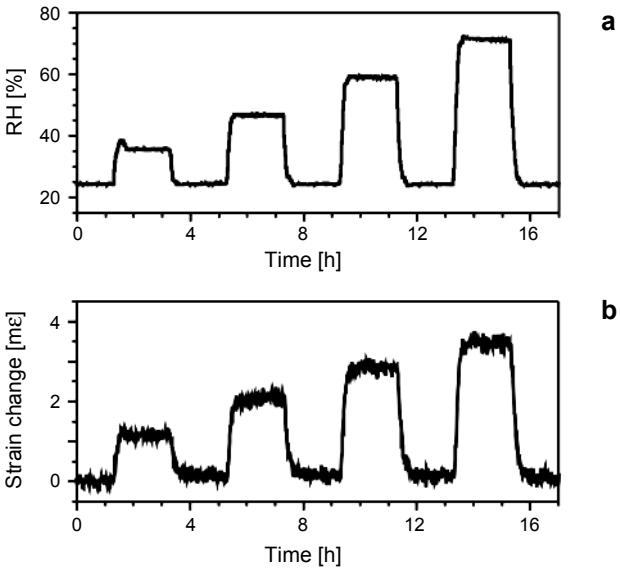

Fig. 10. Temporal evolution of relative humidity (**a**) in the climate chamber and the strain of the test textile fixed along the weft as measured by the cFBG sensor (**b**). The temperature was maintained at 20 °C.

were monitored simultaneously by the cFBG sensor attached with magnetic clamps and by a laser triangulation sensor fixed below the textile.

A laser displacement sensor (Micro-Epsilon LD1605-2) was attached to a bottom part of a metal frame with mounted textile and it was positioned at the center of the loading bar (see Fig. 9). The distance between the sensor and the loading bar was about 24 mm. During experiment triangulation sensor performed the non-contact measurements of the displacement of loading bar with accuracy of 5 μm at the rate of 1 kHz.

Figure 10 shows the strain in the test textile as measured by the cFBG signals (corrected for the fiber interference assuming constant Young's modulus of the textile) while varying the RH. The measurements were taken over a period of 18 hours in 2-hour cycles. Any change of RH in the chamber results in a change of the strain in the textile due to the water vapor adsorption or desorption. The strain measured with the cFBG correlates well with the laser triangulator measurements (see Fig. 11) with a correlation factor of 0.78. This discrepancy can be explained mostly by large uncertainties in Young's modulus of the textile, which depends on the sample

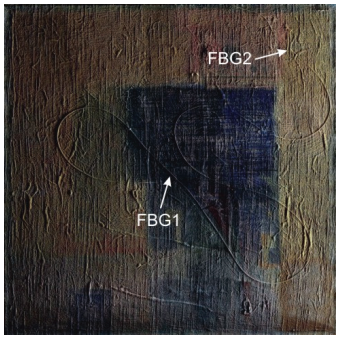

◀ Fig. 11. The model painting on canvas with embedded cFBG sensors.

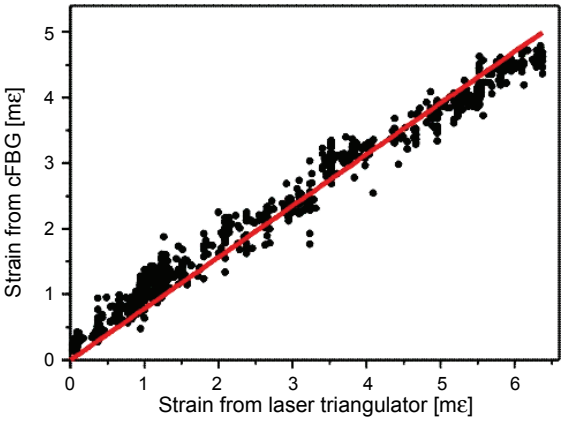

Fig. 12. Strain variations of the test textile as registered by the cFBG sensor versus strain measured by the laser triangulator. The straight line is a linear fit with a slope of 0.78.

and varies with relative humidity [7]. In the RH range studied, Young's modulus for wool decreases with humidity (by about 10%); therefore, corrections to strain measurements by the cFBG are the larger the higher RH. This may explain the slightly nonlinear character of the dependence presented in Fig. 12.

4.4. Application of FBG sensors for measurement of strain in paintings on canvas

In order to demonstrate the usefulness of FBG sensors to monitor strains in paintings on canvas, a model of acrylic painting was prepared by conservator using standard techniques and materials. The selection of acrylic paint was based on general feature that it can become very brittle below 10 °C and thus it is very susceptible even to very small deformations [8]. The canvas was stretched on a wooden stretcher and pre-sized with acrylic preparatory layer from Talens. After application of the first layer an optical fiber was laid on the surface. When the surface was dry, the fiber was covered with a second layer of the same preparatory layer. The object was cured in room conditions for one month before testing. The surface was then painted using acrylic paints. The model painting with two embedded uncoated FBGs sensors – one in the upper-right corner and the other in the center is shown in Fig. 11.

The mechanical response of the painting was studied during normal road transport between two museums maintaining standard precautions for such objects, as proper packing, air suspension system of the track, *etc*. The results of this investigation are shown in Fig. 13, where the upper and the lower curves correspond to strain variations measured in the corner and in the center of the painting, respectively. Both curves reveal rapid- and slow-varying components. The first one is directly related to

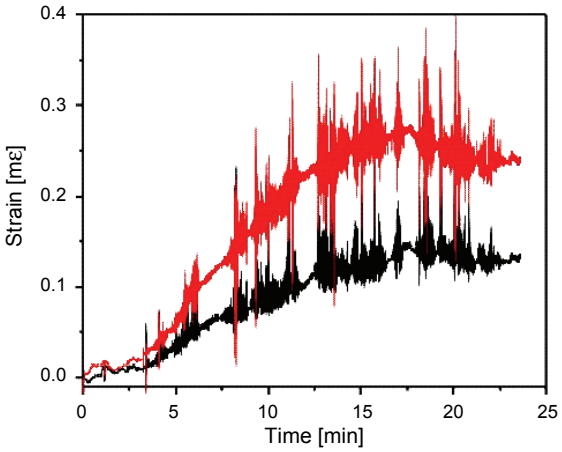

Fig. 13. Strain measured in the corner (the upper curve) and in the center (the lower curve) of the model painting on canvas during road transport.

vibrations in the canvas due to transport; whereas the second is the result of strain transfer from the wooden frame to the canvas. The strain in the canvas slowly increases in response to the expansion of the frame, caused by slight difference in relative humidity between the museum and the truck. It is evident that strain in the corner of the canvas is larger than in the center, as explained in [9]. It is also worth noting that strains associated with changes in the surrounding climate can exceed those induced by shocks during transportation.

To confirm the results obtained with the cFBG sensors, another experiment was performed during road transport. Strain variations in the test painting on canvas were measured simultaneously by the cFBG sensor and by means of the laser triangulator.

Triangulator sensor (Micro-Epsilon ILD 1401-100) was attached to a light metal mounting-system from Bosch clamped to a stretcher and positioned at the center of the rear face of the painting. The laser-to-canvas distance was about 10 cm. The sensor performed the non-contact measurements of the out-of-plane displacement of canvas with accuracy of 200 μm at the rate of 1 kHz. The strain variations were calculated by comparison between length of canvas oscillating in M_{00} mode of amplitude measured by laser sensor with its initial length of 50 cm. The canvas was assumed to oscillate in M_{00} mode. Further details on measuring method and data analysis can be found in [10].

A comparison of in-plane deformations measured directly by cFBG and deformations calculated from out-of-plain distortions measured by laser triangulator is

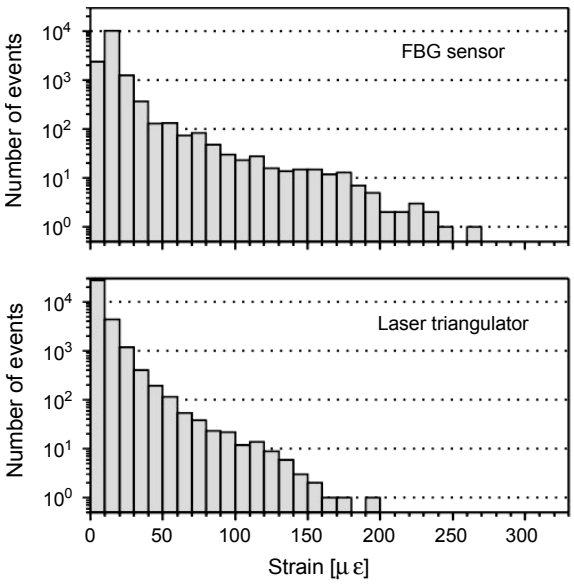

Fig. 14. Strain amplitudes detected by the FBG and the laser triangulator in the model painting on canvas during road transport.

presented in Fig. 14. The results of two independent measurements are in good agreement, which proves that connection between optical fiber and painted canvas is strong and fiber is not sliding during the measurement.

Although the method using FBGs is invasive to the paintings and cannot be applied to real paintings on canvas, it is of great practical importance. The results for models can help in risk assessment for real objects during transport and, since they are of local character, they can identify the most endangered places in the canvas.

5. Conclusions

In this work, the performance of silica fiber Bragg gratings (FBG) as strain sensors in historic textiles and paintings on canvas was studied. Fibers with a ceramic coating were selected for strain investigations in textiles due to their almost perfect strain transfer and much shorter relaxation times compared to acrylic-coated fibers. Fibers were attached to the fabrics in a non-destructive manner using specially designed magnetic clamps. The local strain measured by the cFBG sensors was always consistent with global strains measured using either an UTM or the laser triangulator under variable external force or microclimate conditions. However, strain magnitudes measured by the different methods were comparable only after corrections were made for the influence of fiber on the textile being studied. The fiber effect, directly related to fiber rigidity compared to the individual threads of the textile, can be minimized by using wider magnetic clamps. However, this will reduce the locality of measurements by the FBG.

Strain measurements in model paintings on canvas were carried out using uncoated fibers embedded into the canvas with acrylic preparatory layer from Talens. Although the results given by the FBG directly correspond to deformations in the canvas, the use of these sensors is rather limited to the model paintings due to the invasive manner of their attachment.

Despite some drawbacks, FBG sensors were found very useful in monitoring strain in historic textiles and for assessing environmental risks in these works-of-art.

Acknowledgments – This research was supported by a grant from Iceland, Liechtenstein and Norway through the European Economic Area Financial Mechanism.

References

[1] YE C.C., DULIEU-BARTON J.M., CHAMBERS A.R., LENNARD F.J., EASTOP D.D., *Condition monitoring of textiles using optical techniques*, Key Engineering Materials **413–414**, 2009, pp. 447–454.

[2] YE C.C., DULIEU-BARTON J.M., WEBB D.J., ZHANG C., PENG G.D., CHAMBERS A.R., LENNARD F.J., EASTOP D.D., *Applications of polymer optical fibre grating sensors to condition monitoring of textiles*, Journal of Physics: Conference Series **178**, 2009, article 012020.

[3] HARBACH N.G., *Fiber Bragg Gratings in Polymer Optical Fibers*, PhD Thesis, École Polytechnique Fédérale de Lausanne, 2008.

[4] MELTZ G., MOREY W.W., GLENN W.H., *Formation of Bragg gratings in optical fibers by a transverse holographic method*, Optics Letters **14**(15), 1989, pp. 823–825.
[5] BLACKET D.R., LARGE M., ARGYROS A., *High strain sensing with mPOF and long period gratings*, Proceedings of the 3rd International Workshop Microstructured Polymer Optical Fibre, 2009.
[6] HOWARD R.N., *The Physics of Glassy Polymers*, Applied Science Publishers, Ltd., London, 1978.
[7] MATSUMOTO K., KIM W.-S., LEE K.-B., *Toughness of textile fibers*, Journal of the Textile Machinery Society of Japan **42**, 1996, pp. 66–71.
[8] MECKLENBURG M., *Determining the Acceptable Ranges of Relative Humidity And Temperature in Museums and Galleries Part 2, Structural Response to Temperature*, Report of Museum Conservation Institute, The Smithsonian Institution, Washington, 1998.
[9] FUSTER LOPEZ L., *Estudio de la idondeidad de las masillas de relleno en el tratamiento de lagunas en pintura sobre lienzo*, PhD Dissertation, Universidad Politecnica de Valencia, Spain, 2005.
[10] LASYK Ł., ŁUKOMSKI M., BRATASZ Ł., KOZŁOWSKI R., *Vibration as a hazard during the transportation of canvas paintings*, [In] *Conservation and Access: Contributions to the London Congress 15–19 September 2008*, [Eds.] D. Saunders, J.H. Townsend, S. Woodcock, The International Institute of Conservation of Historic and Artistic Works, London, 2008, pp. 64–68.

Received September 20, 2011
in revised form January 4, 2012